

# Pathways to faceting of vesicles

Mark J. Bowick\* and Rastko Sknepnek†  
*Department of Physics and Soft Matter Program,  
 Syracuse University, Syracuse, New York 13244, USA*

The interplay between geometry, topology and order can lead to geometric frustration that profoundly affects the shape and structure of a curved surface. In this commentary we show how frustration in this context can result in the faceting of elastic vesicles. We show that, under the right conditions, an assortment of regular and irregular polyhedral structures may be the low energy states of elastic membranes with spherical topology. In particular, we show how topological defects, necessarily present in any crystalline lattice confined to spherical topology, naturally lead to the formation of icosahedra in a homogeneous elastic vesicle. Furthermore, we show that introducing heterogeneities in the elastic properties, or allowing for non-linear bending response of a homogeneous system, opens non-trivial pathways to the formation of faceted, yet non-icosahedral, structures.

## I. INTRODUCTION

Although most of the lipid bilayer vesicles found in biological systems are smooth one often observes faceted structures as well. Prominent examples in nature are the protein capsids of many large viruses, the protein-enclosed bacterial organelles known as carboxysomes<sup>1</sup> and the square-shaped bacteria found in saturated brine pools.<sup>2</sup> On the experimental side faceted forms are found in small phosphatidylcholine vesicles below the freezing temperature,<sup>3</sup> some cationic vesicles,<sup>4,5</sup> cross-polymerized vesicles,<sup>6</sup> vesicles assembled from a mixture of anionic and cationic amphiphiles,<sup>5,7,8</sup> vesicles formed from block copolymers with liquid-crystalline side chains,<sup>9–11</sup> giant fullerenes,<sup>12</sup> and gold nanocages.<sup>13</sup> While diverse in their structure, all these systems share the common feature of possessing pathways to lower the total energy by forming stable facets. Over the past four decades substantial research effort has been devoted to understanding the shapes of smooth vesicles. Only recently has there been a growing interest in developing a theoretical understanding of faceted structures with their sharp edges and singular vertices.

To understand the origin of faceting it is essential to understand the physics of smooth vesicles. Early in evolution it became clear that to construct complex life it was necessary to be able to hierarchically compartmentalize and separate different parts of an organism. The compartmentalization was achieved with the aid of vesicles made of molecularly-thin membranes. Biological membranes are typically phospholipid bilayer structures embedded with a variety of membrane and transmembrane proteins.<sup>14</sup> The membrane thickness is typically  $\sim 5\text{nm}$  while the lateral dimensions range from hundreds of nanometers to microns. Given this large aspect ratio such membranes can be treated as quasi-two-dimensional. Vesicular mem-

branes are not limited, however, to biological systems. Nanometer-sized and micron-sized containers can be constructed in the laboratory using lipid molecules,<sup>15,16</sup> block-copolymers<sup>17</sup> and even, as in the case of gold nanocages, inorganic compounds.

While the detailed structure and function of biological membranes is exceedingly complex and still to be fully understood, much insight into their physical properties can be gained by constructing simple mesoscopic models. Helfrich,<sup>18</sup> in a seminal paper, argued that the quasi-two-dimensional nature of membranes implies that their dominant deformation is bending, corresponding to changing shape in space. He constructed a free energy functional that relates the bending energy to the integral of the square of the mean curvature,  $H$ , and to the Gaussian curvature,  $K$ , i.e.

$$E_{bend} = \int dS \left[ 2\kappa (H - H_0)^2 + \kappa_G K \right], \quad (1)$$

where  $H_0$  is the spontaneous curvature and  $\kappa$  and  $\kappa_G$  are respectively the bending and Gaussian rigidities which themselves depend on the molecular details. The Helfrich free energy describes fluid membranes with free lateral diffusion as there is no energy cost for shear deformations. Fluidity is important for biological membranes as it ensures that small apertures formed by transmembrane transport, or from damage of some kind, can be closed quickly. It also allows structural reorganizations within the membrane itself, as seen, for example, in lipid rafts.<sup>19</sup>

Homogeneous fluid vesicles are typically smooth since molecules quickly rearrange themselves to remove any stress that would be generated by the formation of sharp corners or edges. Sharp structures correspond to regions with very high or diverging curvature<sup>20</sup> and are therefore energetically costly. While in real systems the divergence is cut off at some molecular length scale, the energy penalty for forming sharp bends is comparable to molecular en-

ergies and far exceeds the energy cost ( $\sim k_B T$ ) of long-wavelength undulations. To form sharp structures, therefore, there must be a mechanism that either reduces the energy cost associated with the formation of bends or that inhibits the flow of molecules or imposes additional “in-vesicle” order (e.g. liquid crystalline) that would select a non-smooth underlying geometry. The first mechanism can be achieved by introducing asymmetry in the composition of the two leaflets of the bilayer induced by a phase segregation of the two molecular species, thus resulting in local non-zero spontaneous curvature<sup>21</sup> or by segregating excess amphiphiles along long ridges and inducing a spontaneous curvature that is commensurate with the dihedral angle between two faces.<sup>7,22</sup> In this paper we discuss mechanisms that lead to faceting of elastic vesicles. An interesting account of faceting of giant vesicles in the rippled gel phase  $P_{\beta'}$  by osmotic deflation has recently been given by Quemeneur, *et al.*<sup>23</sup>

This paper is organized as follows. In Section II A we discuss pathways to the faceting of elastic membranes that describe viral capsids or bilayer systems cooled below the gelation transition or for which the molecules are cross-polymerized (i.e. tethered to each other). In particular, we show, in Section II A, how topological defects can act as the seeds of buckling to icosahedra, thus providing a simple explanation for the observation that viruses with icosahedral symmetry are spherical for small sizes but well-faceted icosahedra for larger sizes. In Section II B we show how the presence of elastic inhomogeneities also can lead to faceting to regular and irregular polyhedra quite different from icosahedra. Finally, in Section II C, we argue that faceting can also occur in homogeneous elastic vesicles if one allows for a non-linear bending response in terms of a critical curvature.

## II. FACETING OF ELASTIC MEMBRANES

### A. Buckling into icosahedra

One of the hallmarks of viruses is the regular structure of their capsids. The unit building blocks of capsids are capsomeres, robust protein complexes,  $\approx 10\text{nm}$  in diameter, that tile the entire capsid in a regular (crystalline) array. The lattice structures of icosahedral viruses can be described in terms of pairs of non-negative integers,  $(p, q)$  that form a  $T$ -number,  $T = p^2 + q^2 + pq$ .<sup>24</sup> The existence of a lattice combined with the spherical topology is at the center of the argument for size-driven buckling into icosahedra. To properly explain the mechanism behind this buckling phenomenon we need first to

briefly review the complex question of the existence of long-range order on curved surfaces.

Constructing a regular lattice in the plane (or any other flat surface) is straightforward. The simplest example is the ground state of identical point-like particles in an external confining potential interacting via long range repulsive interactions, e.g. identical charges confined to a planar region. The ground state is a triangular lattice with each particle having exactly six equidistant nearest neighbors and a lattice spacing that is determined by the density. Such a state is not frustrated and is stress free. This is no longer the case when one attempts a similar construction on the 2-sphere (the surface of a ball in  $\mathbb{R}^3$ ). Any attempt to map a regular lattice on to the surface of a 2-sphere will result in excess particles. In order to build a smooth covering of the 2-sphere it is necessary, in other words, to remove parts of the original planar lattice. As a result, even in the ground state any crystalline lattice on a 2-sphere will necessarily have a finite number of sites that have coordination different from six, i.e. so called topological defects. Starting from Euler’s polyhedral formula, which states that for any polyhedron  $V - E + F = \chi$ , where  $V$  is the number of vertices,  $E$  is the number of edges,  $F$  is the number of faces, and  $\chi$  is the Euler characteristic of the polyhedron, one can show that the total number of vertices of a crystalline lattice on a sphere has to satisfy the following relation:<sup>25</sup>  $\sum_z (6 - z) N_z = 6\chi = 12$ . Here  $N_z$  is the total number of sites with coordination  $z$  and we have explicitly used that  $\chi = 2$  for a 2-sphere. If we restrict ourselves to coordination numbers  $z = 5, 6$  or  $z = 7$  (physically coordination numbers are near 6), the configuration with the lowest number of defects on a sphere has  $N_5 = 12$ , i.e. twelve five-fold coordinated sites embedded in a regular triangular lattice. We note that, somewhat counterintuitively, this configuration is not always the ground state of the system as shown by Bowick, *et al.*<sup>26</sup> For sufficiently large total number of particles, and reasonable defect core energies, the total energy can be lowered by forming pairs of five- and seven-fold defects that emanate from each of the twelve five-fold coordinated sites. In the following discussion we will ignore this complication and assume that only twelve five-fold defects are present.

Despite their appearance five-fold disclination defects are not local since they owe their existence to removing whole sections of a planar lattice so that it conforms to a 2-sphere. As such they are endowed with considerable elastic energy. To estimate how the elastic energy of a disclination depends on its size we assume that it is surrounded by a Hookean elastic medium. The elastic energy of a two-dimensional crystal is<sup>27</sup>  $E_{el} = \int d^2r A^{ijkl} u_{ij} u_{kl}$ ,

where  $u_{ij}(\vec{r}) = \frac{1}{2}(\partial_i u_j + \partial_j u_i + \partial_k u_i \partial_k u_j)$  is the strain tensor field, with  $u_i(\vec{r})$  ( $i = 1, 2$ ) being the components of the displacement field, and  $A^{ijkl}$  is the material-dependent elastic tensor. For a hexagonal lattice, the elastic tensor has only two independent components,<sup>27</sup> i.e. two Lamé coefficients  $\mu$  and  $\lambda$  and the elastic energy simplifies to<sup>27</sup>

$$E_{el} = \frac{1}{2} \int d^2\vec{r} \left( \lambda (u_{ii})^2 + 2\mu u_{ij} u_{ij} \right), \quad (2)$$

and we assume summation over pairs of repeated indices.

A planar five-fold disclination defect can be constructed by removing a  $60^\circ$  wedge of a triangular lattice and sewing the two cut edges together. A detailed calculation<sup>28</sup> finds that the stretching energy of a five-fold disclination is  $E_{el}^{5-fold} = (Y/32\pi) R^2$ , where  $Y$  is the two-dimensional Young's modulus and  $R$  is the system size.

If the disclination is allowed to buckle out of the plane it can lower its energy by forming a conical structure with the apex at the disclination. In this case the stretching energy is relieved at the expense of a bending penalty. The bending penalty is given by<sup>28,29</sup>

$$E_{bend} = \int dS (2\kappa H^2 + \kappa_G K). \quad (3)$$

It can be shown<sup>28</sup> that the bending energy of such a conical structure is  $E_{bend}^{(5)} \approx (\pi/3) \kappa \log(R/R_b) + \frac{1}{32\pi} Y R_b^2$ , where  $R_b \approx \sqrt{154\kappa/Y}$ . By comparing the expressions for the stretching and bending energies it is clear that for small radii stretching energy is smaller than bending energy and the disclination will remain flat at the expense of stretching its surrounding. As  $R$  increases, the logarithm grows less rapidly than  $R^2$  and it becomes energetically favorable to buckle into a cone. A detailed calculation<sup>28</sup> shows that the buckling transition occurs when the dimensionless ratio, the so-called Föppl-von Kármán or FvK number,  $\gamma = \frac{Y R^2}{\kappa} \gtrsim 154$ .

Another consequence of their non-local character is that disclination defects, much like charges, exert long-range forces on each other. This long-range force is transmitted via the elastic deformation of the medium with the speed of sound playing the role of the speed of light in electrostatics. Disclinations with the same topological charge ( $s = 1$  for a five-fold defect) repel each other. On a 2-sphere, therefore, disclinations adopt a configuration that maximizes their separation; this is the icosahedron for twelve defects.<sup>26</sup>

Moving from planar to spherical geometry does not change the functional forms of the stretching and bending energies but it does renormalize the

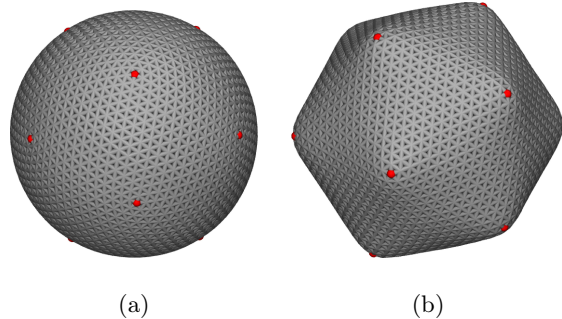


Figure 1: The transition is triggered if the dimensionless FvK number  $\gamma$  exceeds a critical value  $\gamma \sim 10^2$ .<sup>30</sup> Simulated structures are constructed using the  $(p, q) = (12, 3)$  icosadeltahedral triangulation with  $\approx 2 \times 10^3$  vertices and radius  $R \approx 11.5l_0$ , with  $l_0 = 1$  being the average lattice spacing. (a)  $\gamma \approx 170$  and (b)  $\gamma \approx 3500$ . Red dots designate five-fold defects. All snapshots are generated with the Visual Molecular Dynamics (VMD) package<sup>31</sup> and rendered with the Tachyon ray-tracer.<sup>32</sup> Disclination-driven buckling into an icosahedron is discussed in Ref. 30. Results of that study are reproduced here for completeness.

numerical prefactors due to partial screening of the strain induced by the non-zero Gaussian curvature of the sphere.<sup>26</sup> As in the planar case, therefore, the onset of buckling depends solely on the relative strengths of the stretching and bending energies. Since the stretching energy grows rapidly with the radius of the sphere, all defects buckle simultaneously into cones once a critical radius is reached and an icosahedral vesicle is formed.<sup>30</sup> In Fig. 1 we show the shape of the shell below and above the buckling transition. The transition is not sharp but rather a rounded smooth crossover, with vesicles having FvK number  $\gamma \lesssim 150$  being spherical, for  $200 \lesssim \gamma \lesssim 1500$  being noticeably buckled, and for  $\gamma \gtrsim 2000$  being very sharp. For extremely large FvK numbers ( $\gamma \gtrsim 10^7$ ) the vesicle is non-extensible and one observes characteristic ridge-like structures with very interesting scaling properties, e.g.  $E_{ridge}/\kappa \sim \alpha^{7/3} (Y L^2/\kappa)^{1/6}$ , where  $\alpha$  is the angle of the ridge and  $L$  is its length.<sup>33,34</sup>

Finally we note that imposing internal pressure,<sup>35</sup> or a volume constraint,<sup>35,36</sup> shifts the buckling transition to higher values of  $\gamma$  but leaves the basic physics unchanged.

## B. Buckling of multicomponent vesicles

An implicit assumption in the discussion thus far has been that the vesicle is made of an elastically homogenous material. Introducing heterogeneities by allowing for spatially varying Young's modulus

and bending rigidity can lead to alternative buckling mechanisms. The presence of heterogeneities, for example, is believed to be responsible for the structure of the recently synthesized assemblies of oppositely charged amphiphiles.<sup>6,8</sup> The structures observed are  $\sim 100\text{nm}$  bilayer vesicles that are faceted but not icosahedral. SAXS/WAXS measurements combined with atomistic and detailed coarse-grained molecular dynamics simulations have revealed the existence of strongly correlated crystalline domains within the bilayer.<sup>8</sup> A typical domain size was found to be  $\approx 25\text{nm}$ . Simulations show that the crystallographic axes of two neighboring domains are not mutually aligned and that the domains are separated by narrow regions of disordered, or even liquid, amphiphiles. It is reasonable to expect that the bilayer will be softer along those disordered boundary regions. These regions represent grain boundary defects with very different physical properties from the topological defects discussed in the previous section.

To model a vesicle with inhomogeneous elastic parameters we generalize the expressions for stretching (Eq. (2)) and bending (Eq. (3)) energies and allow the two Lamé coefficients and the bending rigidity to depend on the spatial position, i.e.  $\lambda = \lambda(\vec{r})$ ,  $\mu = \mu(\vec{r})$ , and  $\kappa = \kappa(\vec{r})$ . We assume for simplicity that each of these coefficients can take only two values, denoted as “hard” and “soft” and loosely corresponding to strongly correlated facets and grain boundary regions, respectively.

The elasticity theory of thin objects is non-linear<sup>37</sup> and if one allows for spatially varying elastic parameters (even if they have a simple binary distribution) it quickly becomes analytically intractable. We therefore turn to numerical simulations. The vesicle is represented as a discrete triangulated surface. In the case of modeling viral capsids, the vertices of the triangulation correspond to individual capsomeres. If the constitutive units are smaller, as in the case of amphiphilic vesicles, the triangulation can be thought of as a coarse-graining scheme that assigns discrete elements to patches of actual molecules. Each patch is large enough to contain a sufficient number of microscopic degrees of freedom that molecular details are of no importance, but small enough to be considered homogeneous.

On a triangular lattice the simplest form of the discrete stretching energy for a multicomponent system is obtained if we assume that the neighboring sites are connected to each other with harmonic springs with spatially-dependent spring constants  $\varepsilon_{ij}$  and a uniform rest length  $l_0$ <sup>28</sup>

$$\tilde{E}_{el} = \frac{1}{2} \sum_{\langle i,j \rangle} \varepsilon_{ij} (l_{ij} - l_0)^2, \quad (4)$$

where  $l_{ij} = |\vec{r}_i - \vec{r}_j|$  is the Euclidean distance be-

tween two sites at  $\vec{r}_i$  and  $\vec{r}_j$ , respectively,  $\varepsilon_{ij} \in \{\varepsilon_{hard}, \varepsilon_{soft}\}$ , and the sum is carried out over all pairs of nearest neighbors. It is convenient to set  $l_0 = 1$  and use it as the unit of length.

A proper discretization of the bending energy is more complicated with a number of different approaches having been proposed in the physics, applied mathematics and computer graphics literature.<sup>28,39–42</sup> Different approaches vary in the level of computational complexity and accuracy. For the present discussion it is sufficient to adopt the simple discretization suggested by Seung and Nelson.<sup>28</sup> The discrete bending energy is computed as

$$\begin{aligned} \tilde{E}_{bend} &= \frac{1}{2} \sum_{\langle I,J \rangle} \tilde{\kappa}_{IJ} (\vec{n}_I - \vec{n}_J)^2 \\ &= \sum_{\langle I,J \rangle} \tilde{\kappa}_{IJ} (1 - \cos(\theta_{IJ})), \end{aligned} \quad (5)$$

where  $\theta_{IJ}$  is the angle between the unit-length normals  $\vec{n}_I$  and  $\vec{n}_J$  to the neighboring triangles  $I$  and  $J$ , and  $\tilde{\kappa}_{IJ}$  is the position dependent discrete bending rigidity also chosen from a binary set  $\{\kappa_{hard}, \kappa_{soft}\}$ . The spring constant and the discrete bending rigidity are related to the Young’s modulus and the bending rigidity of the continuum theory by  $Y = 2\varepsilon/\sqrt{3}$ <sup>28</sup> (with Poisson ratio  $\nu = 1/3$ ) and  $\kappa = \sqrt{3}\tilde{\kappa}/2$ .<sup>28,43</sup>

We also need to specify which element of the discrete mesh carries which type of information. We note that discrete version of both stretching and bending energies are most naturally defined on edges, i.e. stretching energy is modeled by assigning a linear elastic spring to each edge and bending energy is proportional to the dihedral angle between two neighboring triangles sharing an edge. One is therefore tempted to assign component types to edges. While possible, this is not the most convenient approach as either a vertex or a triangle, and not an edge, is a natural discrete representation of an infinitesimal area element in the continuum description. Defining a discrete form of line tension energy, as discussed below, is also exceedingly hard for component types assigned to edges. We opt rather for defining component types on vertices. In this case a vertex  $i$  is assumed to carry a half-spring with a spring constant  $\varepsilon_i$  which is connected in series to the half-spring of its neighbor  $j$  with a spring constant  $\varepsilon_j$ . The spring constant of the edge ( $ij$ ) is then given by  $\varepsilon_{ij}^{-1} = \varepsilon_i^{-1} + \varepsilon_j^{-1}$ . For the bending energy we choose to define the bending rigidity of an edge as the arithmetic mean of the bending rigidities assigned to its vertices, i.e.  $\kappa_{ij} = (\kappa_i + \kappa_j)/2$ . There are two side effects of defining components on vertices. First, the spring constant of an edge shared by two vertices of the same type is  $\varepsilon_{ij} = \varepsilon_i/2$ ; and

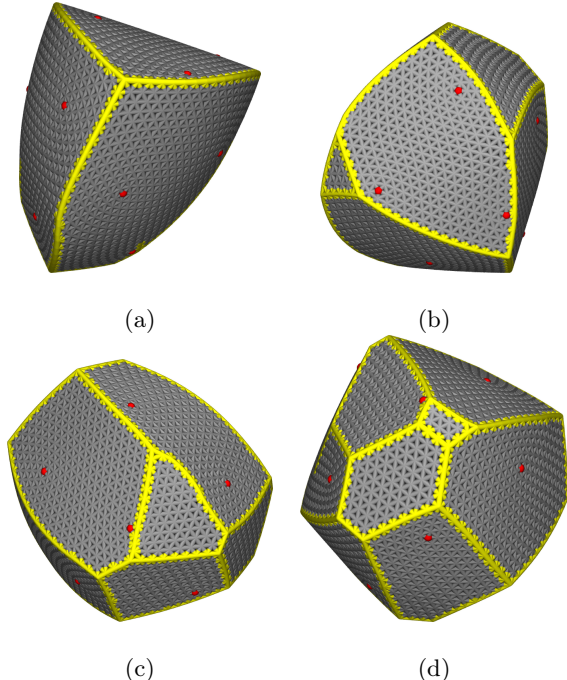


Figure 2: Snapshots of faceted structures with 3% (a), 4% (b), 4.5% (c), and 5% (d) of the soft component (yellow). Twelve five-fold disclination defects are present, as required by the spherical topology, but appear to have no influence on the position of the edges and the size of the facets. A detailed account of faceting of two-component elastic vesicles is presented in Ref. 38 and reproduced here for completeness.

second, while the total number of vertices of a given type is conserved, the vertex-type swaps during the Monte Carlo optimization do not preserve the total number of edge spring constants and bending rigidities. Extensive tests, however, did not reveal any qualitative difference between systems with components defined on edges and systems with components defined on vertices or triangles.

For multicomponent vesicles we require a numerical minimization technique that simultaneously optimizes the position of the individual components as well as the relative population of components. This can be achieved by using stochastic minimization techniques, e.g. the simulated annealing Monte Carlo method. Two components are assigned at random to vertices (or equivalently to edges or triangles) of the initial sphere such that the total fraction of the soft component is  $f$ . A Monte Carlo move has two steps: 1) a vertex is displaced by a vector  $\Delta\vec{r}$  with components chosen at random from a uniform distribution in an interval  $[-\zeta l_0, \zeta l_0]$  (typically,  $\zeta \approx 0.05$ ) followed by 2) swap of types (*soft*  $\leftrightarrow$  *hard*) of a pair of randomly selected vertices. In both steps moves are accepted according to Metropolis rules. During

a simulation, various cooling protocols can be applied such as linear, exponential or power-law. We note that the annealing temperature is not the actual physical temperature but rather a parameter that controls the acceptance rate of the Monte Carlo moves which increase the energy. During the component swap stage the component-type of a vertex (either soft or hard) is preserved so that the total fraction of each component is also constant. Finally we note that the component swap move is purely a convenient simulation tool that allows sampling of the space of component arrangements – it does not correspond to an actual rearrangement of the material within the vesicle which is assumed solid without diffusion. Throughout the simulation the triangulation is preserved – no edge-flip moves<sup>44</sup> that would create or annihilate defects are performed.

The main drawback of the simulated annealing approach is that it typically converges very slowly once a minimum has been approached (for the studied system sizes a minimum is typically reached after  $10^5 - 10^6$  Monte Carlo moves) and there is no guarantee that the obtained structure is a true global minimum, i.e. the ground state configuration. We thus refer to the shapes we obtain as *typical*. On the other hand the experimentally observed shapes may not be true equilibrium shapes either – they are likely to depend in some part on the details of the assembly process.

A detailed study<sup>38</sup> of the shapes of two-component elastic vesicles has found a wide variety of regular and irregular polyhedral shapes, some of which are shown in Fig. 2. If a small amount of soft component is added to an otherwise hard vesicle it arranges into branching lines. As the amount of soft component is increased, these lines start to merge and form facets. Facets are nearly flat with very sharp bends along the soft ridges. The total number of facets increases with the amount of the soft component until a non-universal, size-dependent concentration is reached. Beyond this size-dependent concentration of the soft component it is no longer favorable to generate new facets but instead the soft component is randomly distributed inside the existing ones. Although each configuration still contains twelve five-fold defects, it appears that the size of the facets and the position of the soft ridges is not sensitive to their presence (Fig. 2). We point out that it is possible to entirely remove the residual strain induced by the defects either by appropriately tuning the spring rest lengths<sup>45</sup> or by directly working with reference and realized metrics.<sup>46,47</sup> Such an approach<sup>48</sup> shows that faceting of the soft-hard two-component vesicles occurs even if the defect contribution to the elastic energy is removed.

Thus far we have not assumed any mixing penalty

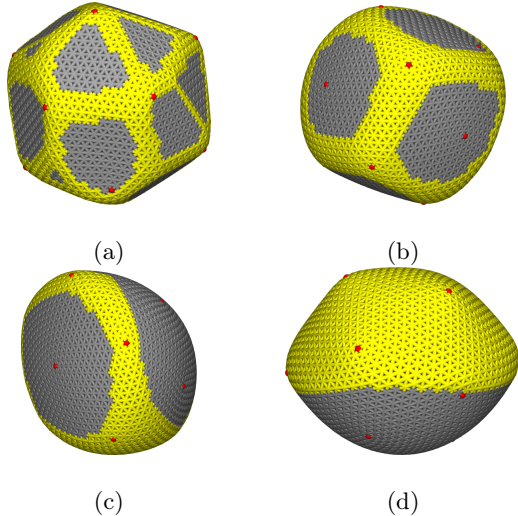


Figure 3: Snapshots of faceted elastic vesicles with various mixing penalties between soft (yellow) and hard (gray) components for a system with an equal number of hard and soft vertices. The mixing penalty increases from (a) to (d). A detailed discussion of the possible phases in two-component elastic vesicles with line tension is given in Ref. 49. The key results of that study are reproduced here for completeness.

for the two components. The components segregated solely as a result of the bending preference. If a mixing penalty, in the form of an effective line tension,  $\Gamma$ , is introduced it competes with the preferred elastic organization of the components and leads to an even richer variety of shapes.<sup>49</sup> In an experimental realization of this system one can envision using the recently discovered linactant molecules,<sup>50–52</sup> which are two-dimensional analogues of surfactants. For weak line tension elasticity dominates and the soft component forms highly bent ridges separating flat hard faces. The width of these soft ridges grows as the line tension increases. If  $\Gamma$  is increased even further the faces start to coarsen and merge together until the components fully separate at  $\Gamma l_0 / \kappa_{hard} \approx 10^{-2}$ ,<sup>49</sup> suggesting that even a small mixing penalty can lead to full phase segregation. A subset of shapes of two-component vesicles with line tension is shown in Fig. 3.

We note that line tension can also lead to very interesting shapes in two-<sup>53</sup> and three-component liquid vesicles.<sup>54</sup>

### C. Faceting due to critical curvature

Some of the faceted shapes observed in experiments, as well as those obtained in simulations (e.g. Fig. 2), show sharp ridges with a large dihedral an-

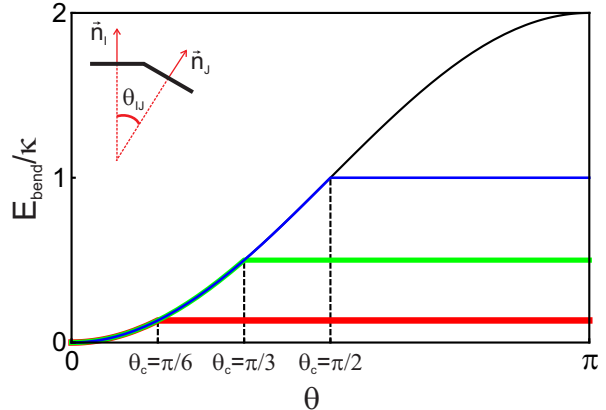


Figure 4: Bending energy (in units of the bending rigidity  $\kappa$ ) as a function of the angle  $\theta$  between unit-length normals to two neighboring triangles without a critical angle (black), with  $\theta_c = \frac{\pi}{6}$  (red), with  $\theta_c = \frac{\pi}{3}$  (green), and with  $\theta_c = \frac{\pi}{2}$  (blue). Inset: Side view of two neighboring triangles  $I$  and  $J$  with their corresponding unit length normals  $\vec{n}_I$  and  $\vec{n}_J$ .

gle between neighboring facets. Once the radius of curvature becomes comparable to the molecular length scales the deformation is no longer locally small and microscopic details of the vesicle start to play a role. Eq. (5) was derived<sup>28</sup> with the assumption that the curvature is smooth and slowly varying between neighboring points, enabling a perturbative expansion of the bending energy in terms of small deviations of the normal vectors to a planar surface. For a locally large deformation this is no longer justifiable and the expression for the bending energy needs to be modified. This is clearly a very hard problem that requires detailed knowledge of the microscopic structure of the vesicle shell. Rather than constructing such a detailed model we make the simple assumption that the bending energy saturates beyond a critical angle. In other words, Eq. (5) is modified to

$$\tilde{E}_{bend}^{crit.} = \tilde{\kappa} \sum_{\langle I, J \rangle} (1 - F(\theta_{IJ})), \quad (6)$$

where

$$F(\theta) = \begin{cases} \cos(\theta) & \text{for } \theta \leq \theta_c \\ \cos(\theta_c) & \text{for } \theta > \theta_c \end{cases} \quad (7)$$

and, as in Eq. (5),  $\theta_{IJ}$  measures the angle between normals to a pair of neighboring triangles and  $\theta_c$  is the critical value of that angle beyond which the bending penalty saturates. A plot of  $\tilde{E}_{bend}^{crit.}$  vs.  $\theta$  is shown in Fig. 4. In this model  $\theta_c$  is treated as an input parameter. In essence,  $\theta_c$  controls the deformation angle beyond which the vesicle shell is sufficiently deformed that atomistic details start to be

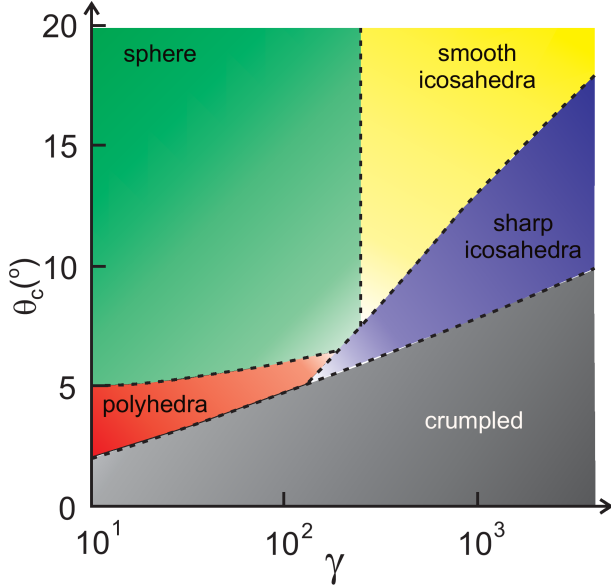


Figure 5: Phase diagram for a vesicle with critical bending angle as a function of the FvK number ( $\gamma$ ) and the value of the critical angle ( $\theta_c$ , shown in degrees). We identify five distinct regimes. In the “sphere” (green) and “smooth icosahedra” (yellow) regimes  $\theta_c$  is large and does not affect the shape. For small  $\gamma$  the vesicle is spherical and crosses over into a smooth icosahedron as  $\gamma$  is increased. At lower values of  $\theta_c$  the presence of a critical angle starts to play a role and the vesicle shape changes substantially. For small  $\gamma$  the elastic energy is completely dominated by the bending contribution and vesicles take irregular polyhedral shapes (red region). For larger values of  $\gamma$  the stretching energy caused by topological defects cannot be ignored and the icosahedral symmetry reemerges, but this time accompanied by sharp ridges (blue region). Finally, for very small values of  $\gamma$  the vesicle is unstable to crumpling (gray).

important. We assume that the vesicle is homogeneous sphere with uniform values for  $\tilde{\kappa}$  and  $\varepsilon$ , and a standard triangular lattice with twelve five-fold defects positioned at the corners of an inscribed icosahedron. While one could argue that the stretching energy should also be modified by introducing a critical edge length beyond which the energy is constant, we use, for simplicity, the expression in Eq. (4) and note that test simulations show that the results are not qualitatively affected by this simplification.

As before, the low energy states were found using simulated annealing Monte Carlo simulations. No constraints on volume or area were imposed. Minimum energy configurations were found after  $\approx 10^6$  Monte Carlo moves using a linear cooling protocol.

We studied vesicles with approximately  $6 \cdot 10^3$  vertices  $((p, q) = (18, 10)$ -chiral;  $(25, 0)$ -achiral) over a range of values of the FvK number ( $\gamma$ ) and critical angle ( $\theta_c$ ). In Fig. 5 we display a phase diagram of

this system mapped with  $\approx 200$  independent pairs of  $\gamma$  and  $\theta_c$ . Five distinct regimes are identified. For low values of  $\gamma$  and moderate to large  $\theta_c$  (green region, denoted as “sphere” in Fig. 5) the bending penalty is too large and vesicles remain spherical. In this region, the angles between normals on any pair of neighboring triangles are smaller than  $\theta_c$  and the existence of an angle cutoff plays no role in determining the shape: we recover the situation discussed in Section II A. If  $\gamma$  is increased, while keeping  $\theta_c$  large, one crosses over into the regime where icosahedral shapes are favorable. Since no deformation exceeds  $\theta_c$  the transition occurs at the same value of  $\gamma$  as in the case without the critical bending angle (yellow region, denoted as “smooth icosahedra” in Fig. 5). If  $\theta_c$  is reduced the existence of an angle cutoff is seen to affect the low energy shapes. In the region where  $\gamma$  is small (red region denoted as “polyhedra” in Fig. 5) one observes irregular polyhedra with sizes and positions of facets and edges that are insensitive to the presence of the five-fold defects. This is to be expected since for small  $\gamma$  the bending penalty completely dominates over stretching and defect-driven buckling into a cone is suppressed. In this region the faceting mechanism is similar to buckling of the soft component as discussed in the previous section. As  $\gamma$  is increased topological defects start to play a role and the system transitions to the regime where defects drive buckling. With a relatively small value of  $\theta_c$ , however, the system can further lower its energy by forming sharp edges that emanate from the defects. This region is denoted as “sharp icosahedra” (blue in Fig. 5). We note that the direction of the sharp edges appears to depend on the details of the triangulation and thus is not universal. Finally, if  $\theta_c$  is too small the vesicle becomes unstable and crumples (gray region denoted as “crumpled” in Fig. 5). In this region the simulations often fail to converge and instead get locked in high-energy states that often occur in the early stages of a simulation. In Fig. 6 we show typical low energy configurations in each of the five regimes.

We point out that this is a toy model with very little ingredients of an actual system. Therefore, all conclusions should be taken as qualitative with very little to no quantitative bearing for real experimental systems such as lipid vesicles. However, we believe that some general qualitative conclusions can still be deduced. For example, it is natural to ask which experimental systems could follow bending mechanism described by this model. We note that for the continuum model to be applicable the deformation has to be small at molecular length scales. In a lipid vesicle, on the other hand, the angular difference between the long axes of two neighboring molecules should be sufficient (a few degrees) for the non-linear

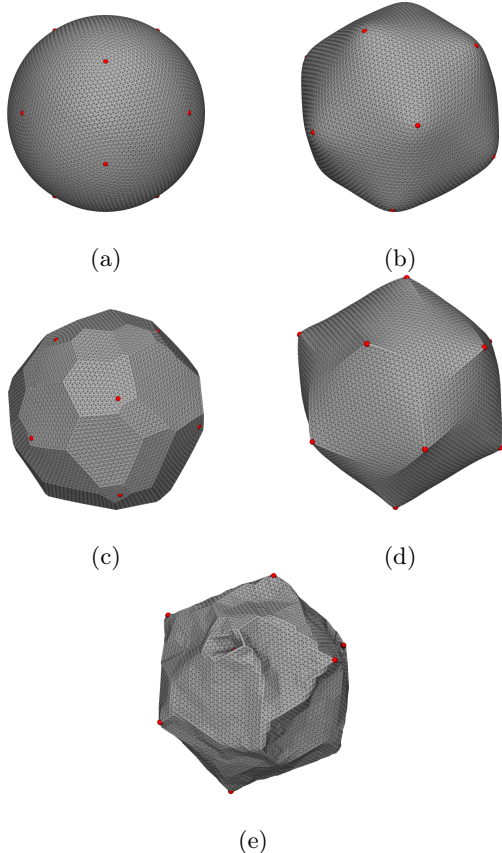


Figure 6: Snapshots of the low energy configurations of a vesicle constructed using  $(p, q) = (18, 10)$   $T$ -number triangulation with  $\approx 6 \times 10^3$  vertices and radius  $R \approx 20.5l_0$ . (a) For low a FvK number  $\gamma \approx 50$  and a large critical angle  $\theta_c = 20^\circ$  the vesicle remains spherical. (b) For  $\gamma \approx 10^3$  and  $\theta_c = 20^\circ$  one observes a smooth buckled structure with icosahedral symmetry akin to the shapes discussed in Section II A. (c) For small  $\gamma \approx 60$  and small  $\theta_c = 5^\circ$  we find an irregular polyhedral vesicle with facets being insensitive to the position of the defects. (d) As FvK number if increased to  $\gamma \approx 10^3$  and the critical angle set to  $\theta_c = 14^\circ$  the structure is icosahedral but with sharp ridges emanating for each defect. (e) Finally, at  $\gamma \approx 2.5 \cdot 10^3$  and very small critical angle,  $\theta_c = 2^\circ$  the vesicle is no longer stable and crumples. Red points indicate positions of twelve five-fold defects.

effects to be appreciable. It is reasonable to expect such conditions to be met for vesicles in the sub  $100nm$  size range as are most of those for which faceting has been reported.<sup>3,6,8</sup>

### III. SUMMARY AND CONCLUSIONS

We have shown that faceted structures can be low energy configurations of elastic vesicles as a result of several different mechanisms. Incompatibility be-

tween crystalline order and spherical topology implies topological defects and residual stress even in the ground state. The stress can be relieved, in part, by buckling into cones seeded at the defects. The buckled structure typically inherits the icosahedral symmetry associated with the defects. This mechanism can qualitatively account for the observation that smaller icosahedral viruses (e.g. *Polyomaviruses*<sup>55</sup>) are smooth (spherical) while larger viruses (e.g. *Mimivirus*<sup>56</sup>) are buckled. For viruses the size of each capsomere is sufficiently large ( $\sim 10nm$ ) that the capsid is a nearly perfect lattice with  $\sim 10^2 - 10^3$  units and no additional defects beyond the minimum twelve five-fold sites required by the topology. In the case of lipid bilayer vesicles lipid molecules are much smaller (occupying an area  $\lesssim 0.5nm^2$ ) and each vesicle is assembled from hundreds of thousands of lipids. If such a vesicle develops crystalline order as a result of cooling or strong electrostatic correlations it is much harder to form a perfect lattice and one instead expects grain boundaries to form. This effect is enhanced by the spherical topology which hinders formation of a uniform crystal to begin with. In the grain boundary region molecules are disordered and may even be in the liquid state. As a result, the shell is expected to be softer. We have shown that, if one allows for the presence of a softer component in an otherwise crystalline vesicle, the low energy configuration can be regular and irregular polyhedra that are not icosahedra. The soft component forms ridges that are highly bent and separate hard flat facets. The faceting mechanism is quite different from the buckling into an icosahedron seeded at the five-fold sites. Furthermore, it is reasonable to expect that the bending response of the vesicle shell is not linear and significantly changes if the local deformation becomes large. We introduced a simple model that takes into account such effects at the most basic level. Even with a such simplified model we were able to show that a non-linearity in the bending response can drastically affect the low energy shapes and lead to interesting faceted structures.

Understanding the mechanisms that lead to the faceting of vesicles goes beyond the realm of an academic exercise and could have far-reaching impact on nano-technology. Flat faces, for example, could be easier to functionalize or otherwise chemically treat. Biochemical reactions are expected to have different rates near flat compared to curved surfaces, which could be utilized to construct highly sensitive transport agents. With the ability to accurately control the shape of vesicles it could be possible to engineer vesicles that would, e.g. selectively target only particular agents. We hope this work will broaden the interest in this emergent subject of modern nano-



science.

This work was supported by NSF grant DMR-0808812. RS would like to thank M. Demers, C. Funkhouser, C. Leung, M. Olvera de la Cruz, L. Palmer, B. Qiao, and G. Vernizzi for collaborations on various aspects of the study of faceting in

multicomponent vesicles as well as to R. Everaers who suggested to analyze the effects of a critical angle bending. RS and MJB also thank the Soft Matter Program at Syracuse University for financial support.

- 
- \* Electronic address: bowick@phy.syr.edu  
 † Electronic address: sknepnek@gmail.com
- <sup>1</sup> C. V. Iancu, D. M. Morris, Z. Dou, S. Heinhorst, G. C. Cannon, and G. J. Jensen, *Journal Of Molecular Biology* **396**, 105 (2010).
  - <sup>2</sup> A. Walsby, *Nature* **283**, 69 (1980).
  - <sup>3</sup> A. Blaurock and R. Gamble, *Journal of Membrane Biology* **50**, 187 (1979).
  - <sup>4</sup> E. Marques, O. Regev, A. Khan, M. da Graca Miguel, and B. Lindman, *Macromolecules* **32**, 6626 (1999).
  - <sup>5</sup> F. Antunes, R. Brito, E. Marques, B. Lindman, and M. Miguel, *The Journal of Physical Chemistry B* **111**, 116 (2007).
  - <sup>6</sup> M. A. Greenfield, L. C. Palmer, G. Vernizzi, M. Olvera de la Cruz, and S. I. Stupp, *Journal of the American Chemical Society* **131**, 12030 (2009).
  - <sup>7</sup> M. Dubois, B. Deme, T. Gulik-Krzywicki, J.-C. Dedieu, C. Vautrin, S. Desert, E. Perez, and T. Zemb, *Nature* **411**, 672 (2001).
  - <sup>8</sup> C. Leung, L. Palmer, B. Qiao, S. Kewalramani, R. Sknepnek, C. Newcomb, M. Greenfield, G. Vernizzi, S. Stupp, M. Bedzyk, et al., *ACS Nano* **6**, 10901 (2012).
  - <sup>9</sup> L. Jia, A. Cao, D. Lévy, B. Xu, P. Albouy, X. Xing, M. Bowick, and M. Li, *Soft Matter* **5**, 3446 (2009).
  - <sup>10</sup> B. Xu, R. Piñol, M. Nono-Djamen, S. Pensec, P. Keller, P. Albouy, D. Lévy, and M. Li, *Faraday discussions* **143**, 235 (2009).
  - <sup>11</sup> L. Jia, D. Lévy, D. Durand, M. Impéror-Clerc, A. Cao, and M. Li, *Soft Matter* **7**, 7395 (2011).
  - <sup>12</sup> L. Lamb, D. Huffman, R. Workman, S. Howells, T. Chen, D. Sarid, and R. Ziolo, *Science* **255**, 1413 (1992).
  - <sup>13</sup> M. Hu, J. Chen, M. Marquez, Y. Xia, and G. V. Hartland, *Journal of Physical Chemistry C* **111**, 12558 (2007).
  - <sup>14</sup> B. Alberts, A. Johnson, J. Lewis, M. Raff, K. Roberts, and P. Walter, *Molecular Biology of the Cell* (Garland Science, New York, 2002).
  - <sup>15</sup> A. Bangham and R. Horne, *Journal of molecular biology* **8**, 660 (1964).
  - <sup>16</sup> S. Veatch and S. Keller, *Biophysical Journal* **85**, 3074 (2003).
  - <sup>17</sup> C. Nardin, T. Hirt, J. Leukel, and W. Meier, *Langmuir* **16**, 1035 (2000).
  - <sup>18</sup> W. Helfrich, *Zeitschrift Fur Naturforschung C-a Journal Of Biosciences* **C 28**, 693 (1973), ISSN 0939-5075.
  - <sup>19</sup> S. Munro, *Cell* **115**, 377 (2003).
  - <sup>20</sup> T. A. Witten, *Rev. Mod. Phys.* **79**, 643 (2007).
  - <sup>21</sup> A. González-Pérez, M. Schmutz, G. Waton, M. Romero, and M. Krafft, *Journal of the American Chemical Society* **129**, 756 (2007).
  - <sup>22</sup> C. A. Haselwandter and R. Phillips, *Phys. Rev. Lett.* **105**, 228101 (2010).
  - <sup>23</sup> F. Quemeneur, C. Quilliet, M. Faivre, A. Viallat, and B. Pépin-Donat, *Physical Review Letters* **108**, 108303 (2012).
  - <sup>24</sup> D. L. D. Caspar and A. Klug, *Cold Spring Harbor Symposia on Quantitative Biology* **27**, 1 (1962).
  - <sup>25</sup> S. Sachdev and D. R. Nelson, *J. Phys. C: Solid State Phys.* **17**, 5473 (1984).
  - <sup>26</sup> M. Bowick, D. Nelson, and A. Travestet, *Physical Review B* **62**, 8738 (2000), ISSN 0163-1829.
  - <sup>27</sup> L. Landau and E. Lifshitz, *Theory of Elasticity* (Butterworth-Heinemann, London, 1995), 3rd ed.
  - <sup>28</sup> H. S. Seung and D. R. Nelson, *Physical Review A* **38**, 1005 (1988).
  - <sup>29</sup> W. Koiter, *A consistent first approximation in the general theory of thin elastic shells: Foundations and linear theory*, pt. 1 (Laboratorium voor Toegepaste Mechanica der Technische Hogeschool, 1959).
  - <sup>30</sup> J. Lidmar, L. Mirny, and D. R. Nelson, *Physical Review E* **68**, 051910 (2003).
  - <sup>31</sup> W. Humphrey, A. Dalke, and K. Schulten, *Journal of Molecular Graphics* **14**, 33 (1996).
  - <sup>32</sup> J. Stone, Master's thesis, Computer Science Department, University of Missouri-Rolla (1998).
  - <sup>33</sup> A. E. Lobkovsky, *Phys. Rev. E* **53**, 3750 (1996).
  - <sup>34</sup> A. E. Lobkovsky and T. Witten, *Physical Review E* **55**, 1577 (1997).
  - <sup>35</sup> A. Siber, *Physical Review E* **73**, 061915 (2006).
  - <sup>36</sup> C. M. Funkhouser, R. Sknepnek, and M. Olvera de la Cruz, *Soft Matter* **9**, 60 (2012).
  - <sup>37</sup> B. Audoly and Y. Pomeau, *Elasticity and Geometry - From Hair Curls to the Non-linear Response of Shells* (Oxford University Press, Oxford, UK, 2010).
  - <sup>38</sup> G. Vernizzi, R. Sknepnek, and M. de la Cruz, *Proceedings of the National Academy of Sciences* **108**, 4292 (2011).
  - <sup>39</sup> K. Brakke, *Experimental Mathematics* **1**, 141 (1992).
  - <sup>40</sup> G. Gompper and D. Kroll, *Journal De Physique I* **6**, 1305 (1996), ISSN 1155-4304.
  - <sup>41</sup> M. Meyer, M. Desbrun, P. Schröder, and A. H. Barr, *Visualization and mathematics* **3**, 34 (2002).
  - <sup>42</sup> E. Magid, O. Soldea, and E. Rivlin, *Computer Vision and Image Understanding* **107**, 139 (2007).
  - <sup>43</sup> B. Schmidt and F. Fraternali, *Journal of the Mechanics and Physics of Solids* **60**, 172 (2012).
  - <sup>44</sup> D. Nelson, T. Piran, and S. Weinberg, *Statistical mechanics of membranes and surfaces* (World Scientific Singapore, 2004), 2nd ed.
  - <sup>45</sup> E. Katifori, S. Alben, E. Cerda, D. R. Nelson, and

- J. Dumais, Proceedings of the National Academy of Sciences **107**, 7635 (2010).
- <sup>46</sup> A. Green and W. Zerna, *Theoretical elasticity* (Dover Pubns, 2002).
- <sup>47</sup> E. Efrati, E. Sharon, and R. Kupferman, Journal of the Mechanics and Physics of Solids **57**, 762 (2009).
- <sup>48</sup> R. Sknepnek and M. Olvera de la Cruz, Physical Review E **85**, 050501 (2012).
- <sup>49</sup> R. Sknepnek, G. Vernizzi, and M. Olvera de la Cruz, Soft Matter **8**, 636 (2012).
- <sup>50</sup> S. Trabelsi, S. Zhang, T. Lee, and D. Schwartz, Physical review letters **100**, 37802 (2008).
- <sup>51</sup> S. Trabelsi, Z. Zhang, S. Zhang, T. R. Lee, and D. K. Schwartz, Langmuir **25**, 8056 (2009).
- <sup>52</sup> S. M. Malone, S. Trabelsi, S. Zhang, T. R. Lee, and D. K. Schwartz, The Journal of Physical Chemistry B **114**, 8616 (2010).
- <sup>53</sup> J. Hu, T. Weikl, and R. Lipowsky, Soft Matter **7**, 6092 (2011).
- <sup>54</sup> M. F. Demers, R. Sknepnek, and M. O. de la Cruz, Physical Review E **86**, 021504 (2012).
- <sup>55</sup> B. Sweet and M. Hilleman, in *Proceedings of the Society for Experimental Biology and Medicine. Society for Experimental Biology and Medicine (New York, NY)* (Royal Society of Medicine, 1960), vol. 105, pp. 420–427.
- <sup>56</sup> B. La Scola, S. Audic, C. Robert, L. Jungang, X. de Lamballerie, M. Drancourt, R. Birtles, J.-M. Claverie, and D. Raoult, Science **299**, 2033 (2003).